

Rotating halo traced by the K giant stars from LAMOST and Gaia

HAO TIAN<sup>1</sup>  
(LAMOST FELLOW)

CHAO LIU,<sup>1</sup> YAN XU,<sup>1</sup> AND XIANGXIANG XUE<sup>1</sup>

<sup>1</sup>*Key Laboratory of Optical Astronomy,  
National Astronomical Observatories, Chinese Academy of Sciences,  
Datun Road 20A, Beijing 100012, PR China;*

(Received December 10, 2018; Revised December 10, 2018; Accepted —)

Submitted to —

ABSTRACT

With the help of Gaia DR2, we are able to obtain the full 6-D phase space information for stars from LAMOST DR5. With high precision of position, velocity, and metallicity, the rotation of the local stellar halo is presented using the K giant stars with  $[\text{Fe}/\text{H}] < -1$  dex within 4 kpc from the Sun. By fitting the rotational velocity distribution with three Gaussian components, stellar halo, disk, and a counter-rotating hot population, we find that the local halo progradely rotates with  $V_T = +27_{-5}^{+4}$  km s<sup>-1</sup> providing the local standard of rest velocity of  $V_{LSR} = 232$  km s<sup>-1</sup>. Meanwhile, we obtain the dispersion of rotational velocity is  $\sigma_T = 72_{-4}^{+4}$  km s<sup>-1</sup>. Although the rotational velocity strongly depends on the choice of  $V_{LSR}$ , the trend of prograde rotation is substantial even when  $V_{LSR}$  is set at as low as 220 km s<sup>-1</sup>. Moreover, we derive the rotation for subsamples with different metallicities and find that the rotational velocity is essentially not correlated with  $[\text{Fe}/\text{H}]$ . This may hint a secular evolution origin of the prograde rotation. It shows that the metallicity of the progradely rotating halo is peaked within  $-1.9 < [\text{Fe}/\text{H}] < -1.6$  without considering the selection effect. We also find a small fraction of counter-rotating stars with larger dispersion and lower metallicity. Finally, the disk component rotates with  $V_T = +182_{-6}^{+6}$  km s<sup>-1</sup> and  $\sigma_T = 45_{-3}^{+3}$  km s<sup>-1</sup>, which is quite consistent with the metal-weak thick disk population.

*Keywords:* galaxies: individual (Milky Way) — Galaxy: kinematics and dynamics — Galaxy: halo — Stars: individual (K-giants)

1. INTRODUCTION

It has been widely accepted that the Milky Way, at least the halo, was formed through hierarchically merging smaller stellar systems, such as globular clusters and dwarf galaxies (Belokurov et al. 2006). With a long time evolving, the stellar members of those merged systems will be continuously stripped and then form stellar streams (Johnston et al. 1999). Such phenomena have been widely searched with photometric sky surveys, e.g. SDSS (York et al. 2000) and Pan-STARRS (Bernard et al. 2016). Since the first stellar stream, Sagittarius

stream, discovered by Ibata et al. (1994), many streams have been discovered with matched filter method (Rockosi et al. 2002; Grillmair & Carlin 2016; Grillmair & Dionatos 2006a,b,c; Grillmair 2009) and other methods (Mateu et al. 2018). But the streams are not the final fate of those merged clusters or dwarf galaxies, a longer evolving time will make the streams more and more relaxed and finally become part of the smoothing halo, i.e. it is not visible in the geometric space (Helmi et al. 1999), even blurred in the phase space (Helmi & Zeeuw 2000; Sanderson et al. 2015).

Assuming those merged stellar systems fell in with random orbits (Sanderson et al. 2015), the contribution of  $z$ -axis angular momentum  $L_z$  overall should be around 0. The net angular momentum is directly related to the merging history, not only including the

Corresponding author: Chao Liu  
liuchao@nao.cas.cn

minor mergers of the globular cluster and dwarf galaxies, such as the Sagittarius Stream, but also including the major merger events, such as the recently discovered Gaia-Enceladus (Helmi et al. 2018), also named *Gaia-Sausage* (Belokurov et al. 2018), which contributes a larger fraction of retrogradely rotating stars. Another possibility is that the merged halo was driven to slowly rotate by the non-axisymmetric structure in the disk (e.g. bar) in a long time scale (Athanasoula et al. 2013).

The studies on dynamics of the halo have been done since 1980s (Frenk & White 1980) who used 66 clusters to constrained the rotation velocity  $60 \pm 26 \text{ km s}^{-1}$ . As the velocity ellipsoid is directly related to the mass distribution of the halo (Binney & Tremaine 2008), more work focused on the distribution of the dispersions (Sommer-Larsen et al. 1997; Sirko et al. 2004; Smith et al. 2009; Hattori et al. 2013; Kafle et al. 2013; Loebman et al. 2018).

Because of the difficulty of observation of proper motions, especially for distant stars. Morrison et al. (1990) studied the kinematics of the halo and disk using the G and K giant stars within 4 kpc from the Sun, and claimed a prograde rotation of  $V_T = 25 \pm 15 \text{ km s}^{-1}$ . They also showed that the metallicity of the thick disk stars can be as low as -1.6. Smith et al. (2009) studied the kinematics of the local halo using  $\sim 1700$  solar neighbourhood subdwarfs and found that the stellar halo exhibits no rotation and the rotational velocity  $V_\phi$  dispersion  $82 \pm 2 \text{ km s}^{-1}$ , what should be noticed is that the typical velocity errors are large, about 30 to 50  $\text{km s}^{-1}$ .

More recently, the progress of the observations and data analysis techniques, high precision proper motions have been obtained through combining catalogues obtained at different epochs cross a long time baseline (Tian et al. 2017; Belokurov et al. 2018). Deason et al. (2017) used the 3D velocity calculated from the proper motion of different tracers, including RR Lyrae, Blue Horizontal Branch (BHB) and K giant stars, in a distant volume from *Gaia* Data Release (*hereafter GDR*) 1 and SDSS dataset to study the halo rotation. A prograde rotation was found with  $V_T = 14 \pm 2 \pm 10 \text{ km s}^{-1}$ . What is more, the metal richer stars are showing a stronger prograde rotation which is explained as a small fraction of halo stars formed *in situ*. Kafle et al. (2017) also found a similar trend with samples of Main Sequence Turnoff and K giant stars only with radial velocity available. What is different is that the metal poorer K giant stars show a retrograde rotation.

Since Carollo et al. (2007) discovered the inner and outer halo and claimed that the inner halo is rotating progradely, in contrast the outer components is rotating retrogradely. But the systematic bias in distance esti-

mates led to a debate (Schönrich et al. 2011; Beers et al. 2012). This will be highly improved by the *Gaia* mission (Perryman et al. 2001).

GDR2 (Gaia Collaboration et al. 2018a,b,c,d,e,f) contains  $\sim 1.3$  billion stars high accuracy proper motions and parallaxes, which have brought a series of amazing results about the halo, such as the velocity determination of globular clusters and rotation curve of the Large Magellanic Cloud (Gaia Collaboration et al. 2018e). Besides, Gaia Collaboration et al. (2018e) also derived a lower limit total mass for the Milky Way.

Guoshoujing Telescope (the Large Sky Area Multi-Object Fiber Spectroscopic Telescope, hereafter LAMOST) is a 4-meter, quasi-meridian, reflecting Schmidt telescope which makes it an efficient spectroscopic telescope (Cui et al. 2012; Deng et al. 2012; Zhao et al. 2012). Liu et al. (2017) and Xu et al. (2018) used metal poor K giants from LAMOST to trace the density profile of the halo and found an inner oblate, outer nearly spherical profile. Recently, LAMOST has released its 5th data (DR5). As low resolution of  $R = 1800$ , the uncertainties of  $T_{\text{eff}}$  and  $[\text{Fe}/\text{H}]$  are typical  $\sim 100 \text{ K}$  and  $\sim 0.1$  dex, respectively, for the stellar spectra with signal to noise ratio larger than 30.

The paper studies the rotation of the local stellar halo using the combination of the GDR2 and LAMOST DR5 K-giant stars and is constructed as follow. In Section 2, the sample stars are selected. The model of the distribution of rotational velocity is developed in Section 3. The results are discussed in Section 4. The conclusions are listed in Section 5.

## 2. DATA SAMPLE

In this work, we use K giant stars selected from LAMOST DR5 based on the criteria suggested by Liu et al. (2014) to study the rotation of the nearby halo. After cross-matching with GDR2, we obtained the parallax, proper motions, radial velocities and metallicities for the tracer stars. A robust metallicity cut with  $[\text{Fe}/\text{H}] < -1$  is used to remove the majority of disk stars, which leaves 6660 K giant stars. In this case most of the thin disk stars and many thick disk stars will be removed. As we will discuss in the following sections, the left disk component will be considered during the analysis. With the distances from Bailer-Jones et al. (2018), the samples within 4 kpc and relative distance error  $D_{\text{error}}/D < 0.2$  are further selected so that the distance estimates are reliable, and 3827 stars are left in the sample. Comparing the radial velocities between GDR2 and LAMOST, we find an offset  $RV_{\text{Gaia}} - RV_{\text{LAMOST}}$  of  $5.38 \text{ km s}^{-1}$ , which was also mentioned by Tian et al. (2015) and Schönrich & Aumer (2017). To avoid this systematics,

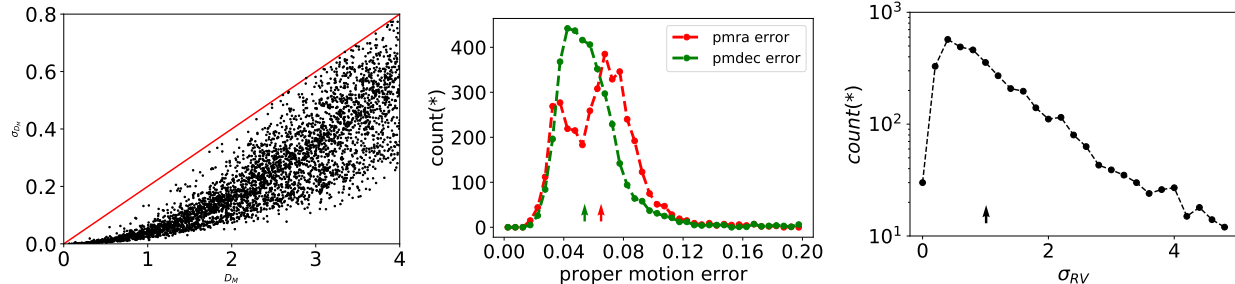


**Figure 1.** Distributions of the errors of proper motions, radial velocities and cylindrical velocities in the left, middle and right panels respectively. The red line in the left panel indicates the limit of the distance error 20%. The arrows indicate the median errors for each quantities.

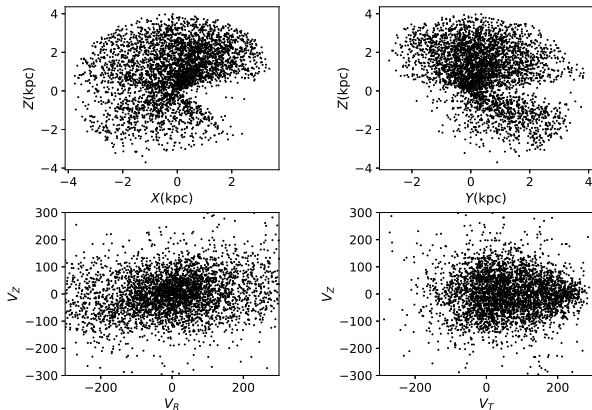


**Figure 2.** Distributions of the sample in geometric space (top panels) and velocity space (bottom panels).

we adopt the radial velocity provided by GDR2. Figure 1 shows the error distributions of distance, proper motions and radial velocity in the left, middle and right panels respectively. We can find that the errors of distance increase with distances. From the middle panel, the median errors of proper motion in *RA* and *DEC* are  $0.065$  and  $0.054$   $\text{mas yr}^{-1}$ , respectively, which are labelled with red and green arrows. The median error of radial velocity is  $1.0$   $\text{km s}^{-1}$  labelled with arrow in the right panel.

We use *galpy* (Bovy 2015) to calculate the 3D locations in heliocentric cartesian coordinates,  $X$ ,  $Y$ ,  $Z$ , and velocity components in galactocentric cylindrical coordinates, radial component  $V_R$ , rotational (azimuthal) component  $V_T$ , and vertical component  $V_Z$ . By default, we adopt the velocity of the local standard of rest (LSR) with respect to the Galactic center as  $V_{LSR} = 232$   $\text{km s}^{-1}$  (McMillan 2017) and the solar motion with respect to the LSR as  $(U_{\odot}, V_{\odot}, W_{\odot}) = (11.1, 12.24, 7.25)$   $\text{km s}^{-1}$  (Schönrich et al. 2010).

Figure 2 shows the distributions of the selected K giant stars in geometric (top panels) and velocity (bottom panels) spaces. The samples do not show disk-like features, implying that most of the disk stars are removed

by the cut in  $[\text{Fe}/\text{H}]$ . The top panels show that the stars are rarely sampled at  $X > 0$ ,  $Y > 0$ , and  $Z \sim 0$ , which is caused by the observational limit of LAMOST survey. This would not affect the detection of the rotation of the halo. The bottom-left panel shows that the distribution in  $V_R$  versus  $V_Z$  space is quite smooth. And the bottom-right panel displays an excess with  $V_T$  at around  $200$   $\text{km s}^{-1}$ , which may be the slight contamination of the thick disk.

In Figure 3, no obvious correlation between  $[\text{Fe}/\text{H}]$  and  $R_{GC}$  is found. The colors of the dots indicate the distance errors, which also show no significant correlation with  $[\text{Fe}/\text{H}]$ . This implies that the samples do not experience any selection bias in metallicity.

In the middle panel, the distribution of the rotation velocity  $V_T$  versus metallicity  $[\text{Fe}/\text{H}]$  is shown with the gray dots. Clearly we find that more stars are progradely rotating in the metal richer side, which is suggested to be the disk component. The black lines in the blue and red shades are the rotation velocity for the halo and disk components respectively, which will be discussed in the later sections.

In the right panel, the errors of the velocities are shown, which are calculated following the calculation of Johnson & Soderblom (1987). The median errors of  $V_R$ ,  $V_T$  and  $V_Z$  are  $5.4$ ,  $11.3$  and  $4.3$   $\text{km s}^{-1}$  as represented by the red, green and blue arrows, respectively.

### 3. MODEL OF THE DISTRIBUTION OF $V_T$

In Figure 4, it is seen that the distribution of  $V_T$  for the samples (black dots with error bars) shows two peaks and a long tail beyond  $V_T < -200$   $\text{km s}^{-1}$ . This hints that it may contain three components, The most dominated component shows up a peak located just at the right side of  $V_T = 0$ . The second component contributes a metal-rich peak at around  $200$   $\text{km s}^{-1}$ . And the third one, maybe a broad one, contributes to the long tail at  $V_T < -200$   $\text{km s}^{-1}$ , especially at metal poor end. By convenience, we assume all the three components are Gaussians and their distribution of  $V_T$  can be defined as

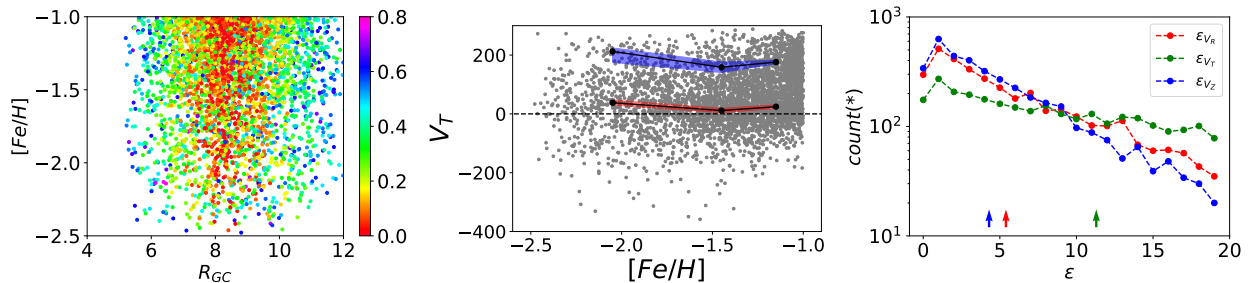


**Figure 3.** Left panel: The distribution of stars in  $R_{GC} - [Fe/H]$  plane with color-coded distance error. Middle panel: The rotational velocity distribution of the K giant stars is shown as the gray dots. The black solid lines in the blue and red shaded regions indicate the rotational velocities of the disk and halo components, respectively. The shadow colors from heavy to light represent the uncertainties from  $1\sigma$  to  $3\sigma$ . Right panel: The distribution of the errors of three velocity components. The red, green and blue arrows indicate the median errors for  $V_R$ ,  $V_T$  and  $V_Z$ , respectively.

$$p_i(V_T^{(k)}|f_i, V_{T,i}, \sigma_i, \epsilon^{(k)}) = \frac{f_i}{\sqrt{2\pi(\sigma_i^2 + \epsilon_k^2)}} \exp\left(-\frac{(V_T^k - V_{T,i})^2}{2(\sigma_i^2 + \epsilon_k^2)}\right), \quad (1)$$

where  $i = 1, 2, 3$  represent for the three components,  $f_i$ ,  $V_{T,i}$ , and  $\sigma_i$  stand for the fraction, mean velocity, and velocity dispersion for the  $i$ th component, respectively.  $\epsilon_k$  is the error of  $V_T$  for  $k$ th star. According to Bayes' theorem, the posterior probability distribution of the unknown parameters can be written as

$$p(\theta_1, \theta_2, \theta_3|V_T) \propto \prod_{k=1}^n \sum_{i=1}^3 p_i(V_T|\theta_i, \epsilon^{(k)}) p(\theta_1, \theta_2, \theta_3), \quad (2)$$

where  $\theta_i = (f_i, V_{T,i}, \sigma_i)$  is the parameter vector for the  $i$ th component.  $k$  represents for the  $k$ th star in the samples with totally  $n$  stars. We adopt simplistic and loose uniformly distributed priors such that  $0 < f_i < 1$ ,  $-100 < V_{T,1} < 100 \text{ km s}^{-1}$ ,  $100 < V_{T,2} < 300 \text{ km s}^{-1}$ ,  $-200 < V_{T,3} < 0 \text{ km s}^{-1}$ , and  $\sigma_i < 200 \text{ km s}^{-1}$ . We further requires  $f_1 + f_2 + f_3 = 1$  so that  $f_3$  is not a free parameter but derived from  $f_1$  and  $f_2$ . Therefore, we totally have 8 free parameters in the model, i.e.  $f_1$ ,  $f_2$ ,  $V_{T,1}$ ,  $V_{T,2}$ ,  $V_{T,3}$ ,  $\sigma_{T,1}$ ,  $\sigma_{T,2}$ , and  $\sigma_{T,3}$ .

Then we apply *emcee* (Foreman-Mackey et al. 2013) to run a Markov Chain Monte Carlo (MCMC) simulation with Affine solver for Eq. (2) with 2000 burn-in iterations. Figure 5 shows the results of the MCMC. We adopt the median values of the MCMC samples as the best-fit parameters and show the best-fit models in the top-left panel of Figure 4. The differences between the median values and the 16% and 84% values are calculated as the upper and lower uncertainties for each parameter. The first row of Table 1 lists the best-fit parameters and their uncertainties of the three Gaussians.

## 4. RESULT

### 4.1. Identification of the three components

The 1st component with  $V_{T,1} = 27_{-5}^{+4} \text{ km s}^{-1}$  and  $\sigma_{T,1} = 72_{-4}^{+4} \text{ km s}^{-1}$  is likely the stellar halo population, since the dispersion is quite similar to Smith et al. (2009) and Bird et al. (2018) at galactocentric distance of 10 kpc. The 2nd component shows quite faster rotation with  $V_{T,2} = 182_{-6}^{+6} \text{ km s}^{-1}$  and smaller dispersion  $\sigma_{T,2} = 45_{-3}^{+3} \text{ km s}^{-1}$ . It is noted that Morrison et al. (1990) claimed that the *metal-weak thick disk* has rotational velocity of  $\langle V_\phi \rangle = 170 \pm 15 \text{ km s}^{-1}$ , Beers et al. (2014) also obtained quite similar values  $\langle V_\phi \rangle = 181 \text{ km s}^{-1}$  with a dispersion  $53 \text{ km s}^{-1}$  and  $\langle V_\phi \rangle = 166 \text{ km s}^{-1}$  with a dispersion  $47 \text{ km s}^{-1}$  using the metal weak thick disk samples selected by Bidelman & MacConnell (1973) and Ruchti et al. (2011) respectively, all of which are quite consistent with our results. Therefore, the second component in our results is believed to be the metal-weak thick disk dynamically. The 3rd component shows retrograde rotation with  $V_{T,3} = -99_{-58}^{+47} \text{ km s}^{-1}$  and larger dispersion of  $124_{-19}^{+23} \text{ km s}^{-1}$ . As we see in Section 4.3, this population has lower metallicity than the other two. It is either the so-called outer halo (Carollo et al. 2007) or an accreted debris in the solar neighborhood. In this work we focus on the stellar halo, i.e. the 1st component.

### 4.2. The rotation of the local stellar halo

The stellar halo with the heliocentric distance of 4 kpc (the 1st component) shows a significant prograde rotation of  $27_{-5}^{+4} \text{ km s}^{-1}$ . Comparing to other works, such rotation is different with the value from Deason et al. (2017) and the value for K giant samples from Kafle et al. (2017). What should be kept in mind is that their samples have no overlapping with ours. Morrison et al. (1990) also studied the halo and disk with K giant stars within 4 kpc and found that the stellar halo with  $[Fe/H] < -1.6$  progradely rotates with  $25 \pm 15 \text{ km s}^{-1}$ , which is quite consistent with ours, while the dispersion

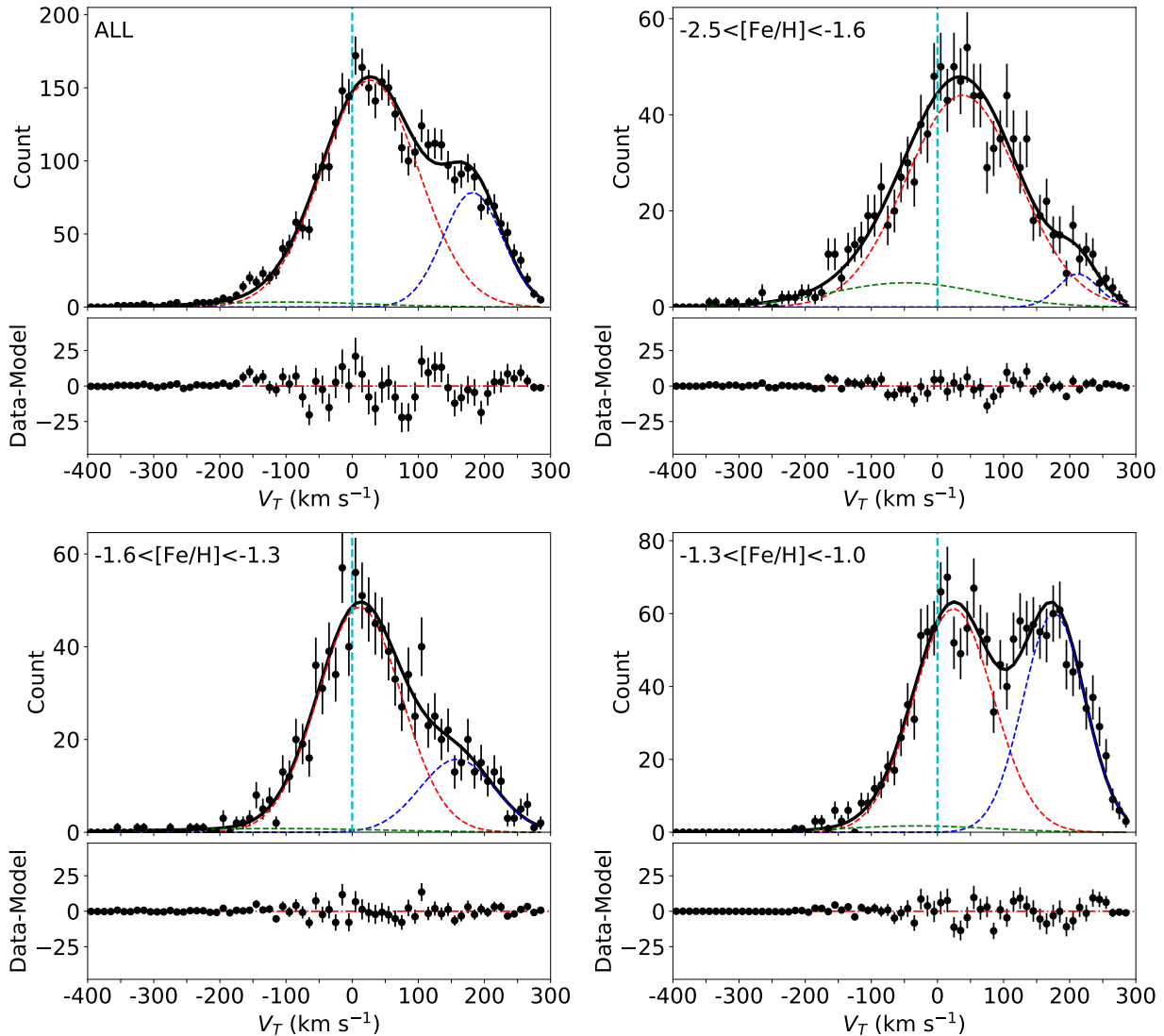


**Figure 4.** The top-left panel shows the distribution of  $V_T$  for all the sample stars (black dots). The error bars are derived from Poisson distribution. The bin size is set at  $10 \text{ km s}^{-1}$ . The red, blue, and green dashed lines indicate the best-fit Gaussian components  $i = 1, 2,$  and  $3$  respectively. The thick black solid line indicates the total distribution of the three-Gaussian model. The lower plot in the panel shows the residual distribution between the data and the model. No significant substructure is found in the residuals. The other panels are similar to the top-left one but for different  $[\text{Fe}/\text{H}]$  bins. From top-right to the bottom-right, the panels show the distribution of  $V_T$  and the corresponding best-fit models with metallicity bins of  $-2.5 < [\text{Fe}/\text{H}] < -1.6$ ,  $-1.6 < [\text{Fe}/\text{H}] < -1.3$ , and  $-1.3 < [\text{Fe}/\text{H}] < -1.0$ , respectively.

they detected is at  $98 \pm 13 \text{ km s}^{-1}$ , slightly larger than this work. Considering the recent work by Belokurov et al. (2018), where the volumes selected overlap with ours, the rotational velocity are quite similar with ours, 20 to  $30 \text{ km s}^{-1}$  in spherical coordinate.

#### 4.3. $V_T$ versus metallicity

Deason et al. (2017) used accurate proper motion to study the rotational velocity of halo stars and argued that the prograde rotation of the metal richer K giants is faster than that of the metal poorer sample. Kafle et al. (2017) also obtained a similar trend, but the difference

is not significant. In light of those works, we detect the rotational velocity for the sub-samples with different metallicities.

We separate the samples into three sub-groups with  $-2.5 < [\text{Fe}/\text{H}] < -1.6$ ,  $-1.6 < [\text{Fe}/\text{H}] < -1.3$ , and  $-1.3 < [\text{Fe}/\text{H}] < -1.0$ . For each sub-sample, similar MCMC simulation is applied and the best-fit 3-Gaussian model parameters are listed in Table 1. The comparison between the observed distributions of  $V_T$  and the models for different metallicities are displayed in Figure 4.

The black line with red shadow in Figure 3 indicates  $V_{T,1}$  as a function of  $[\text{Fe}/\text{H}]$  for the halo population (the

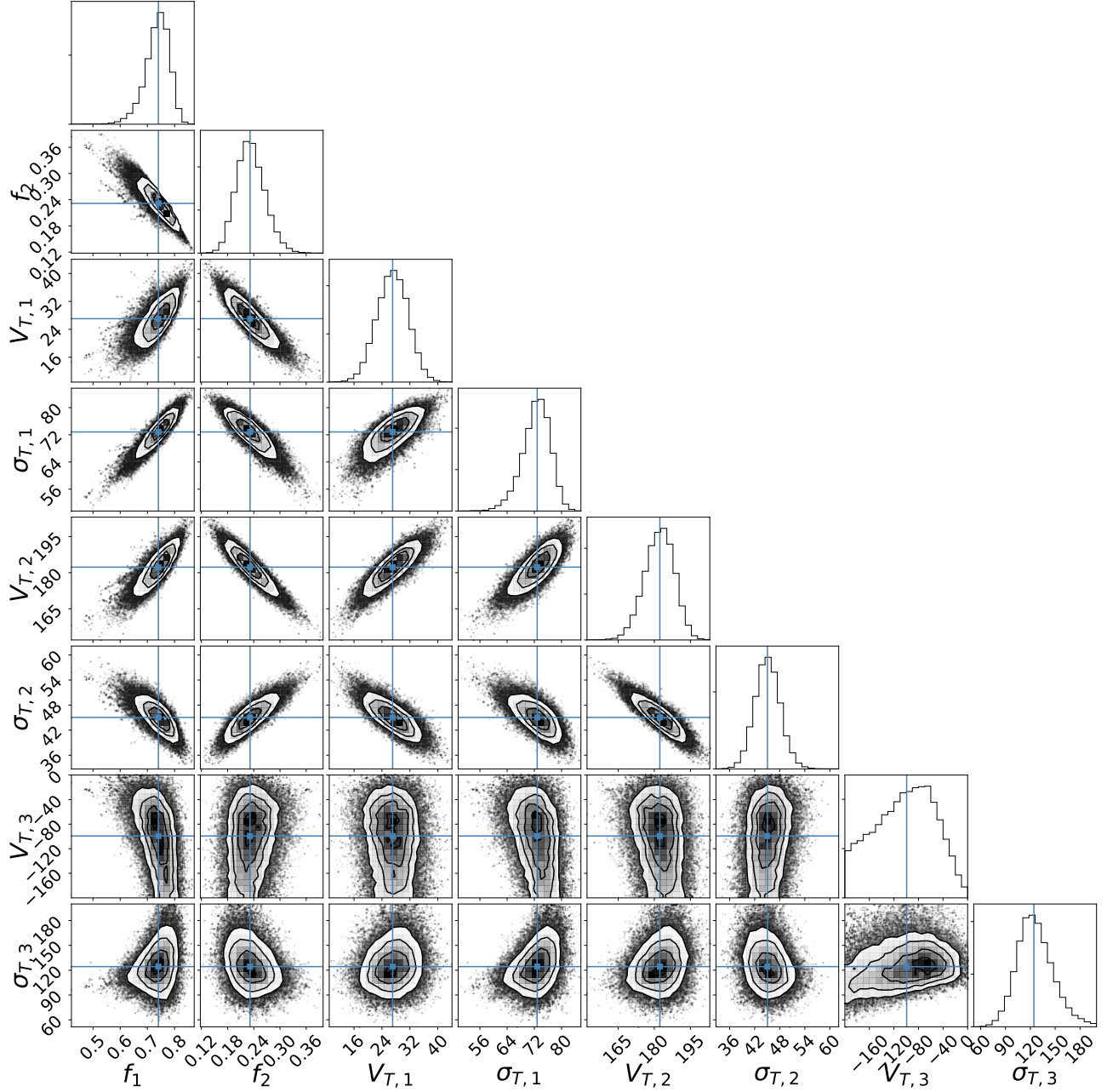


**Figure 5.** The results the MCMC simulation. The correlations of any two parameters are shown in the *corner* plot. The cyan lines are the median values of each individual parameters.

**Table 1.** Best fit parameters of 3-Gaussian Models derived from MCMC.

	$f_1$	$f_2$	$f_3$	$V_{T,1}$ km s <sup>-1</sup>	$\sigma_{T,1}$ km s <sup>-1</sup>	$V_{T,2}$ km s <sup>-1</sup>	$\sigma_{T,2}$ km s <sup>-1</sup>	$V_{T,3}$ km s <sup>-1</sup>	$\sigma_{T,3}$ km s <sup>-1</sup>	$N$
all	$0.741^{+0.038}_{-0.047}$	$0.231^{+0.034}_{-0.030}$	0.028	$27^{+4}_{-5}$	$72^{+4}_{-4}$	$182^{+6}_{-6}$	$45^{+3}_{-3}$	$-99^{+47}_{-58}$	$124^{+23}_{-19}$	3827
$-2.5 < [\text{Fe}/\text{H}] < -1.6$	$0.828^{+0.089}_{-0.164}$	$0.046^{+0.041}_{-0.017}$	0.126	$38^{+9}_{-8}$	$85^{+5}_{-7}$	$212^{+12}_{-37}$	$30^{+21}_{-9}$	$-47^{+32}_{-58}$	$113^{+21}_{-9}$	1134
$-1.6 < [\text{Fe}/\text{H}] < -1.3$	$0.752^{+0.066}_{-0.071}$	$0.217^{+0.068}_{-0.061}$	0.031	$11^{+7}_{-7}$	$63^{+5}_{-5}$	$159^{+18}_{-18}$	$56^{+8}_{-8}$	$-115^{+60}_{-55}$	$158^{+25}_{-26}$	1020
$-1.3 < [\text{Fe}/\text{H}] < -1.0$	$0.550^{+0.058}_{-0.059}$	$0.421^{+0.039}_{-0.043}$	0.029	$24^{+7}_{-6}$	$60^{+7}_{-7}$	$176^{+6}_{-6}$	$47^{+3}_{-3}$	$-31^{+23}_{-52}$	$112^{+25}_{-9}$	1673

1st component). Rather than an increasing rotational velocity with the metallicity argued by previous works, this result prefers to an essentially flat relation between  $V_{T,2}$  and  $[\text{Fe}/\text{H}]$ . In other word, we do not find the rotation of the local stellar halo is substantially correlated with metallicity.

It is worthy to note that the K giant samples used by Deason et al. (2017) are within 50 kpc and  $|z| > 4$  kpc and the samples used by Kafle et al. (2017) are within 17 kpc and  $|z| > 4$  kpc. Neither of them is spacially overlapping with our sample.

The fraction  $f_1$  of the halo population seems also independent of  $[\text{Fe}/\text{H}]$ , as seen in the corresponding column of Table 1. However, we find that  $f_1$  is peaked at  $-2 < [\text{Fe}/\text{H}] < -1.6$ . We find that  $f_1$ , the fraction of the halo population, decreases with metallicity, because of the increasing of the disk population. This again confirms that the first component should be the stellar halo. Note that the selection effect in  $[\text{Fe}/\text{H}]$  is not taken into account.

The black line in the blue shadow in Figure 3 shows rotational velocities at different metallicity bins for the disk component (the 2nd component). It is seen that the uncertainties of  $V_{T,2}$  become smaller at metal richer side. This is because the fraction of the disk becomes larger when  $[\text{Fe}/\text{H}]$  increases, as seen in the column  $f_2$  of Table 1. Thus more stars are involved in this component. This supports that the component has higher metallicity than the halo population.

Finally,  $f_3$  column in Table 1 shows that the counter-rotational component occupies about 12.6% at  $-2.5 < [\text{Fe}/\text{H}] < -1.6$  and only contributes 2.9% at  $-1.3 < [\text{Fe}/\text{H}] < -1.0$ . This means that it is contributed by the most metal-poor stars. The averaged metallicity of the component may be even lower than the halo population. This is consistent with Carollo et al. (2007) that the outer halo has metallicity of  $\sim -2.2$  dex and in counter-rotation.

#### 4.4. Possible mechanism of the prograde rotation of the stellar halo

The flat relationship between  $V_{T,1}$  and  $[\text{Fe}/\text{H}]$  implies that the prograde rotation may not be originated from the sustained angular momenta of the minor mergers, but in favor of an effect of secular evolution. Indeed, Athanassoula et al. (2013) suggested that the rotating bar in the central region of the Galactic disk may transfer angular momenta to the halo. It is also noted that Xu et al. (2018) found the halo is oblate with axis-ratio lower than 0.5 at around 10 kpc, which may be related to the rotation of the halo. It is noted that, from Figure 2 in Helmi et al. (2018) the *Gaia-Enceladus* contributes

a non-ignorable fraction of stars in the local volume, especially with metallicity around -1.5, what's more, almost all of those stars are retrogradely rotating. This indicates that the relatively slower rotation velocity in our results with metallicity between -1.6 and -1.3 might be caused, at least partly, by the major merger event.

#### 4.5. Impact from parameter choices

As the *LSR* velocity brings a directly change in the rotational velocity during the conversion from proper motions, radial velocities and distances, we test the effect of different choices of  $V_{LSR}$ . We select three  $V_{LSR}$  values from literatures, 240  $\text{km s}^{-1}$  (Reid et al. 2014), 232  $\text{km s}^{-1}$  (Schönrich et al. 2010) and 220  $\text{km s}^{-1}$  (Dehnen 2000) for the test. We obtain that  $V_T = 35_{-5}^{+4}$ ,  $27_{-5}^{+4}$ , and  $15_{-5}^{+4}$   $\text{km s}^{-1}$  for  $V_{LSR} = 240$ , 232, and 220  $\text{km s}^{-1}$ , respectively. It is clear that a larger  $V_{LSR}$  leads to a higher halo rotation speed. However, even with the minimum value of  $V_{LSR}=220$   $\text{km s}^{-1}$ , the stellar halo is still in substantially prograde rotation. Moreover, we also find that the rotational velocity is essentially independent of the metallicity with different  $V_{LSR}$ .

## 5. CONCLUSION

We have studied the rotation of the halo with local K giant star samples within 4 kpc. Using the proper motions and radial velocities from *Gaia* and metallicities from LAMOST, we draw the following conclusions.

Firstly, the rotational velocity of the local stellar halo is strongly correlated to the *LSR* speed,  $V_{LSR}$ , and also the azimuthal velocity of the Sun,  $V_{\odot}$ . With  $V_{LSR} = 232$   $\text{km s}^{-1}$  and  $V_{\odot}=12.24$   $\text{km s}^{-1}$ , the halo is progradely rotating with  $V_T = 27_{-5}^{+4}$   $\text{km s}^{-1}$ . The dispersion of  $V_T$  of the halo K giant stars is  $\sigma_{V_T} = 72_{-4}^{+4}$   $\text{km s}^{-1}$ .

Secondly, we find that the rotational velocity of the stellar halo is independent of the metallicity in the local volume, which is different with the results in the outer volume claimed by Deason et al. (2017) and Kafle et al. (2017). The flat relationship between  $V_T$  and  $[\text{Fe}/\text{H}]$  hints that the rotation may be due to secular rotation, rather than due to the net angular momenta from the minor mergers.

Finally, we also identified a metal-poor and counter-rotating hot component with rotational velocity of  $-99_{-58}^{+47}$   $\text{km s}^{-1}$ , which is likely the outer halo. And a disk-like component rotating with  $V_T=182_{-6}^{+6}$   $\text{km s}^{-1}$  is also identified, which is likely the metal-weak thick disk by comparing the results with previous results (Morrison et al. 1990; Beers et al. 2014).

This work is supported by the National Key Basic Research Program of China 2014CB845700. CL

acknowledges the NSFC under grants 11873057 and 11333003. The LAMOST FELLOWSHIP is supported by Special Funding for Advanced Users, budgeted and administrated by Center for Astronomical Mega-Science, Chinese Academy of Sciences (CAMS). HT is supported by the Young Researcher Grant of National Astronomical Observatories, Chinese Academy of Science. X.-X Xue thanks the "Recruitment Program of Global Youth Experts" of China and NSFC 11390371. Guoshoujing Telescope (the Large Sky Area Multi-Object Fiber Spectroscopic Telescope LAMOST) is a National Major Scientific Project built by the Chi-

nese Academy of Sciences. Funding for the project has been provided by the National Development and Reform Commission. LAMOST is operated and managed by the National Astronomical Observatories, Chinese Academy of Sciences. This work has made use of data from the European Space Agency (ESA) mission *Gaia* (<https://www.cosmos.esa.int/gaia>), processed by the *Gaia* Data Processing and Analysis Consortium (DPAC, <https://www.cosmos.esa.int/web/gaia/dpac/consortium>). Funding for the DPAC has been provided by national institutions, in particular the institutions participating in the *Gaia* Multilateral Agreement.

## REFERENCES

- Athanassoula, E., Machado, R. E. G., & Rodionov, S. A. 2013, *MNRAS*, 429, 1949
- Bailer-Jones, C. A. L., Rybizki, J., Fouesneau, M., Mantelet, G., & Andrae, R. 2018, arXiv:1804.10121
- Beers, T. C., Carollo, D., Ivezić, Ž., et al. 2012, *ApJ*, 746, 34
- Beers, T. C., Norris, J. E., Placco, V. M., et al. 2014, *ApJ*, 794, 58
- Belokurov, V., Zucker, D. B., Evans, N. W., et al. 2006, *ApJL*, 642, L137
- Belokurov, V., Erkal, D., Evans, N. W., Koposov, S. E., & Deason, A. J. 2018, *MNRAS*, 478, 611
- Bernard, E. J., Ferguson, A. M. N., Schlafly, E. F., et al. 2016, *MNRAS*, 463, 1759
- Bidelman, W. P., & MacConnell, D. J. 1973, *AJ*, 78, 687
- Binney, J., & Tremaine, S. 2008, *Galactic Dynamics: Second Edition*, by James Binney and Scott Tremaine. ISBN 978-0-691-13026-2 (HB). Published by Princeton University Press, Princeton, NJ USA, 2008.
- Bird, S. A., Xue, X.-X., Liu, C., et al. 2018, arXiv:1805.04503
- Carollo, D., Beers, T. C., Lee, Y. S., et al. 2007, *Nature*, 450, 1020
- Bovy, J. 2015, *ApJS*, 216, 29
- Cui, X.-Q., Zhao, Y.-H., Chu, Y.-Q., et al. 2012, *Research in Astronomy and Astrophysics*, 12, 1197
- Deason, A. J., Belokurov, V., Koposov, S. E., et al. 2017, *MNRAS*, 470, 1259
- Dehnen, W. 2000, *AJ*, 119, 800
- Deng, L.-C., Newberg, H. J., Liu, C., et al. 2012, *Research in Astronomy and Astrophysics*, 12, 735
- Foreman-Mackey, D., Hogg, D. W., Lang, D., & Goodman, J. 2013, *PASP*, 125, 306
- Frenk, C. S., & White, S. D. M. 1980, *MNRAS*, 193, 295
- Gaia Collaboration, Eyer, L., Rimoldini, L., et al. 2018, arXiv:1804.09382
- Gaia Collaboration, Helmi, A., van Leeuwen, F., et al. 2018, arXiv:1804.09381
- Gaia Collaboration, Katz, D., Antoja, T., et al. 2018, arXiv:1804.09380
- Gaia Collaboration, Spoto, F., Tanga, P., et al. 2018, arXiv:1804.09379
- Gaia Collaboration, Babusiaux, C., van Leeuwen, F., et al. 2018, arXiv:1804.09378
- Gaia Collaboration, Brown, A. G. A., Vallenari, A., et al. 2018, arXiv:1804.09365
- Grillmair, C. J. 2009, *ApJ*, 693, 1118
- Grillmair, C. J., & Carlin, J. L. 2016, *Tidal Streams in the Local Group and Beyond*, 420, 87
- Grillmair, C. J., & Dionatos, O. 2006, *Bulletin of the American Astronomical Society*, 38, 48.03
- Grillmair, C. J., & Dionatos, O. 2006, *ApJL*, 643, L17
- Grillmair, C. J., & Dionatos, O. 2006, *ApJL*, 641, L37
- Hattori, K., Yoshii, Y., Beers, T. C., Carollo, D., & Lee, Y. S. 2013, *ApJL*, 763, L17
- Helmi, A., White, S. D. M., de Zeeuw, P. T., & Zhao, H. 1999, *Nature*, 402, 53
- Helmi, A., & de Zeeuw, P. T. 2000, *MNRAS*, 319, 657
- Helmi, A., Babusiaux, C., Koppelman, H. H., et al. 2018, *Nature*, 563, 85
- Ibata, R. A., Gilmore, G., & Irwin, M. J. 1994, *Nature*, 370, 194
- Johnson, D. R. H., & Soderblom, D. R. 1987, *AJ*, 93, 864
- Johnston, K. V., Zhao, H., Spergel, D. N., & Hernquist, L. 1999, *ApJL*, 512, L109
- Kafle, P. R., Sharma, S., Lewis, G. F., & Bland-Hawthorn, J. 2013, *MNRAS*, 430, 2973
- Kafle, P. R., Sharma, S., Robotham, A. S. G., et al. 2017, *MNRAS*, 470, 2959
- Liu, C., Xu, Y., Wan, J.-C., et al. 2017, *Research in Astronomy and Astrophysics*, 17, 096
- Liu, C., Deng, L.-C., Carlin, J. L., et al. 2014, *ApJ*, 790, 110

- Loebman, S. R., Valluri, M., Hattori, K., et al. 2018, *ApJ*, 853, 196
- Mateu, C., Read, J. I., & Kawata, D. 2018, *MNRAS*, 474, 4112
- McMillan, P. J. 2017, *MNRAS*, 465, 76
- Morrison, H. L., Flynn, C., & Freeman, K. C. 1990, *AJ*, 100, 1191
- Perryman, M. A. C., de Boer, K. S., Gilmore, G., et al. 2001, *A&A*, 369, 339
- Reid, M. J., Menten, K. M., Brunthaler, A., et al. 2014, *ApJ*, 783, 130
- Rockosi, C. M., Odenkirchen, M., Grebel, E. K., et al. 2002, *AJ*, 124, 349
- Ruchti, G. R., Fulbright, J. P., Wyse, R. F. G., et al. 2011, *ApJ*, 737, 9
- Sanderson, R. E., Helmi, A., & Hogg, D. W. 2015, *ApJ*, 801, 98
- Schönrich, R., Binney, J., & Dehnen, W. 2010, *MNRAS*, 403, 1829
- Schönrich, R., Asplund, M., & Casagrande, L. 2011, *MNRAS*, 415, 3807
- Schönrich, R., & Aumer, M. 2017, *MNRAS*, 472, 3979
- Sirko, E., Goodman, J., Knapp, G. R., et al. 2004, *AJ*, 127, 914
- Smith, M. C., Evans, N. W., Belokurov, V., et al. 2009, *MNRAS*, 399, 1223
- Sommer-Larsen, J., Beers, T. C., Flynn, C., Wilhelm, R., & Christensen, P. R. 1997, *ApJ*, 481, 775
- Tian, H.-J., Liu, C., Carlin, J. L., et al. 2015, *ApJ*, 809, 145
- Tian, H.-J., Gupta, P., Sesar, B., et al. 2017, *ApJS*, 232, 4
- Xu, Y., Liu, C., Xue, X.-X., et al. 2018, *MNRAS*, 473, 1244
- York, D. G., Adelman, J., Anderson, J. E., Jr., et al. 2000, *AJ*, 120, 1579
- Zhao, G., Zhao, Y.-H., Chu, Y.-Q., Jing, Y.-P., & Deng, L.-C. 2012, *Research in Astronomy and Astrophysics*, 12, 723